SUPPORTING INFORMATION TO

$BaCoO_2$ with tetrahedral coordination: The Missing Element to understand Energy Storage and Conversion Applications in $BaCoO_{3-\delta}$-based-Perovskite

A. Diatta[1], C. V. Colin[2], R. Viennois[1], M. Beaudhuin[1], J. Haines[1], P. Hermet[1], A. van der Lee[3], L. Konczewicz[4,5], P. Armand[1] and J. Rouquette[1]

1. *ICGM, Univ Montpellier, CNRS, ENSCM, 34095 Montpellier, France*

2. *Institut Néel, CNRS and Université Grenoble Alpes, BP166, F-38042 Grenoble Cedex 9, France*

3. *IEM, Univ Montpellier, CNRS, ENSCM, Montpellier, France*

4. L2C, Univ Montpellier, CNRS, Montpellier, France

5. Institut of High Pressure Physics, Polish Academy of Sciences, Sokołowska 29/37, 01-142 Warsaw, Poland.

Structural Information

Cubic or hexagonal perovskite?

The ABO_3 ideal perovskite oxides adopt the cubic $Pm\bar{3}m$ structure in which *A* is the large cation (*A* = Ba, Sr, Mg, La, Sr, …) and *B* the small one (*B* = Co, Cr, Cu, Fe, Mn, …). In this simple structure, the *B*-cation is at the center of oxygen octahedra whereas *A*-cation is twelve-fold coordinated with the oxygen anions resulting in a corner-sharing octahedral framework, Fig. S1a. In this ideal structure *A*-site and *B*-site exhibit 2+/3+ and 4+/3+ oxidation state in order to respect electro neutrality. One can already note that oxygen non stoichiometry $ABO_{3-\delta}$ can easily be created by using combinations of different oxidation states in such a structure for the *A*- and the *B*-sites. The crystal structure depends on the cation and anion ionic radii according to the Goldschmidt tolerance factor *t*, which defines the deviation from the ideal cubic perovskite structure[1]:

$$t = \frac{r_A + r_O}{\sqrt{2}(r_B + r_O)}$$

r_A, r_B and r_O are the respective ionic radii from the *A*, *B* and *O* atoms

The cubic perovskite structure is favored for $0.8 < t < 1$ while for $t > 1$ hexagonal perovskite structures are preferred with face-shared BO_6 octahedra to increase the accessible volume for the *A*-site cations.

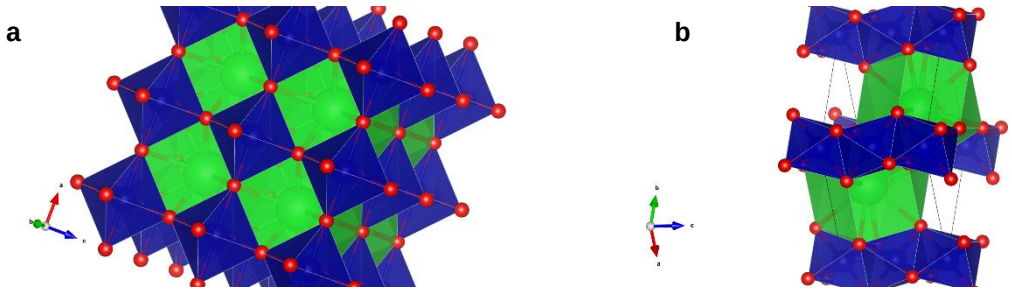

Fig. S1: ABO_3 perovskite structure in the prototype. a) cubic (corner sharing octahedral framework) and b) hexagonal forms (face sharing octahedral framework). *A*, *B* and oxygen atoms are respectively shown using green, blue and red spheres.

$BaCoO_{3-\delta}$ polymorphs with $0 \leq \delta \leq 1$

The $BaCoO_{3-\delta}$ system was described by Raveau et al.[2] and Mentré et al.[3]

$BaCoO_3$ presents the hexagonal 2H-perovskite structure[4], Fig. S1b, with space group $P6_3/mmc$, which is defined by 2-hexagonal BaO_3 stacking sequences and consists of infinite CoO_6 face-sharing oxygen octahedra along ***c***. In such a structure without any oxygen non stoichiometry, Co-oxidation state is purely 4+.

Modifications of this hexagonal perovskite were observed for oxygen-rich systems, Fig. S2a and S2b which correspond to the 12H- hexagonal[5] and 5H- trigonal[6] phases respectively, whereas strongly oxygen-deficient $BaCoO_{2.2}$ cubic structure[3] and the ultimate trigonal $BaCoO_2$ reduced phases[7] were proposed. In the latter case of $BaCoO_2$, unit cell parameters could only be determined and from the similarities between the x-ray powder diffraction patterns, the $BaZnO_2$-type structure[7,8] with the $P3_121$ space group was proposed.

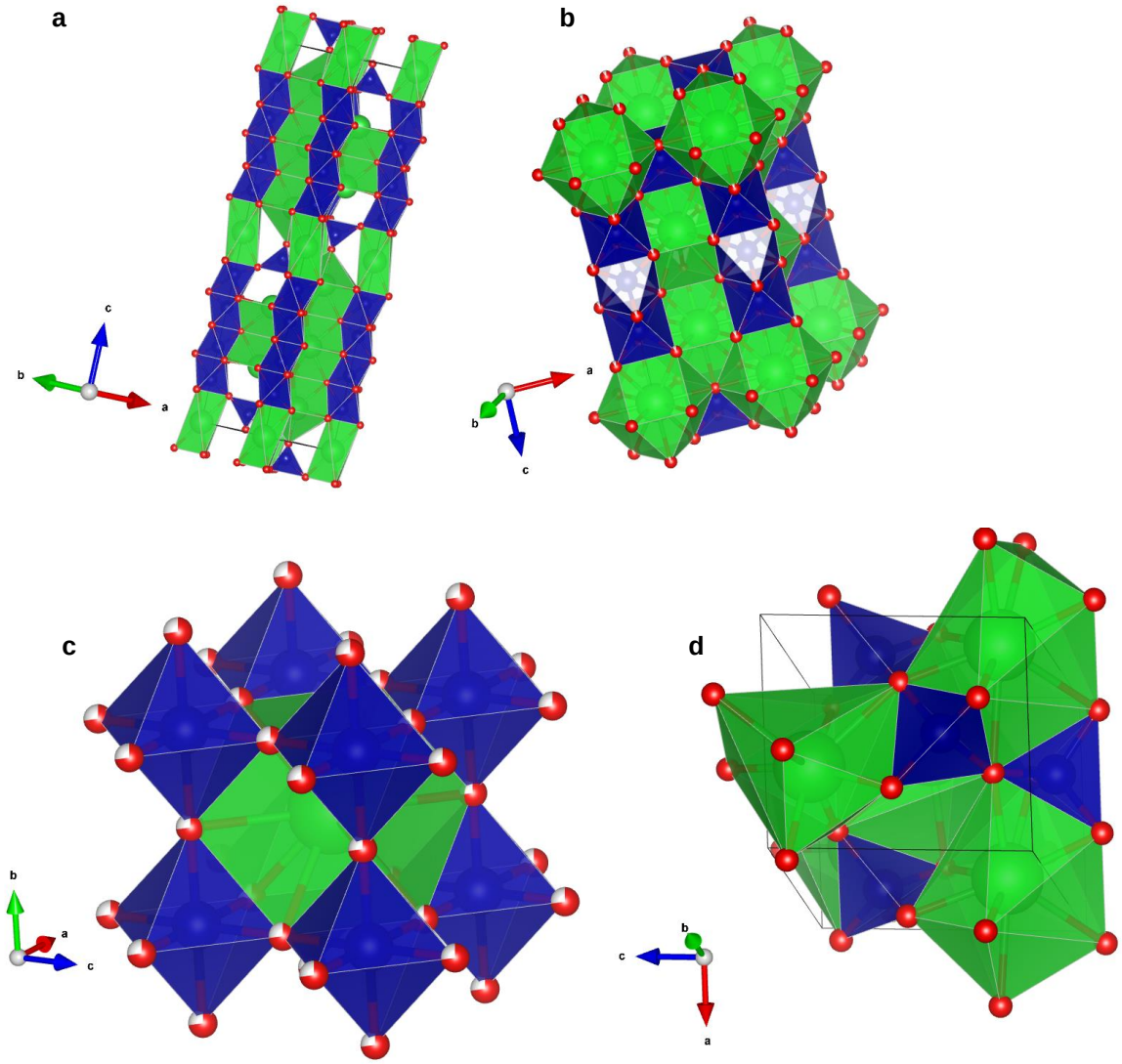

Fig. S2: Reported $BaCoO_{3-\delta}$ polymorphs. Modification of the hexagonal perovskite for oxygen rich-systems: a) $P6_3/mmc$ 12H-$BaCoO_{2.6}$[5] and b) $P\text{-}3m1$ 5H-$BaCoO_{2.8}$ –structures[6]; c)

strongly oxygen-deficient $BaCoO_{2.2}$ cubic $Pm\bar{3}m$ structure[3] and d) trigonal $P3_121$ $BaZnO_2$-type structure[7,8] constituted of cobalt corner- sharing oxygen tetrahedra. Barium, cobalt and oxygen atoms are respectively shown using green, blue and red spheres.

More recently, a tetragonal highly oxygen-deficient metastable phase $BaCoO_{2+\delta}$ with the $P4/mmm$ space group[9] and another $P2_1/m$ monoclinic $BaCoO_{2.67}$[10] form derived from the cubic perovskite structure were also reported, Fig. S3. The latter structure shows three different Co coordination environment, i.e. octahedral, square pyramidal and tetrahedral.

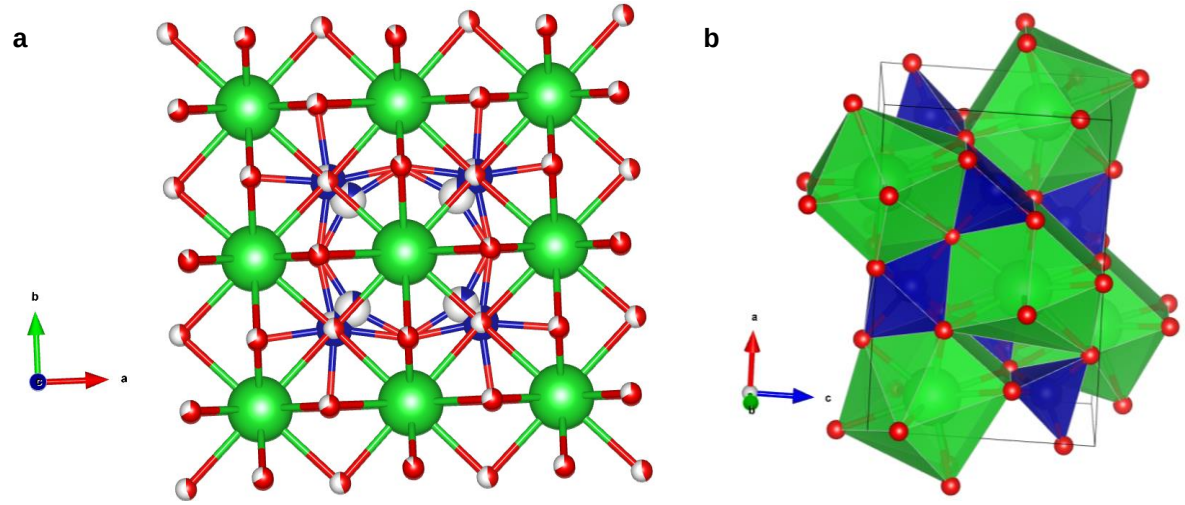

Fig. S3: Recently reported $BaCoO_{3-\delta}$ polytypes. a) highly oxygen-deficient $BaCoO_{2+\delta}$ perovskite $P4/mmm$[9] and b) $P2_1/m$ monoclinic $BaCoO_{2.67}$ perovskite[10] related phases. Barium, cobalt and oxygen atoms are respectively shown using green, blue and red spheres.

Comparison of $BaCoO_2$, $BaZnO_2$ and SiO_2 quartz structures:

$BaCoO_2$ exhibits the $P3_121$ structure as already observed in $BaZnO_2$[7,8]. Both arrangements are derived from the SiO_2 prototype α-quartz structure, which is of high importance in Materials and Earth's Science. The physical properties of α-quartz were found to be directly related to its crystal structure mainly based on the tetrahedral tilting angle (δ) and the $\widehat{SiOSi}$ intertetrahedral bridging angle (θ). δ can be defined as the order parameter of the α-β phase transition of quartz at 847 K, which can be associated with the loss of the piezoelectric properties at high temperature, Fig. S4, i.e. $\delta = 0$ for β quartz, whereas $\theta = 154°$. The $\boldsymbol{c}/\boldsymbol{a}$ unit cell parameter-ratio also provides interesting information on the structure and Table 1 permits to compare the α-, β-quartz, $BaZnO_2$ and $BaCoO_2$ structures. From these data, $BaCoO_2$ exhibits an intermediate compactness between α-quartz and $BaZnO_2$ structure ($BaZnO_2$ being the less dense).

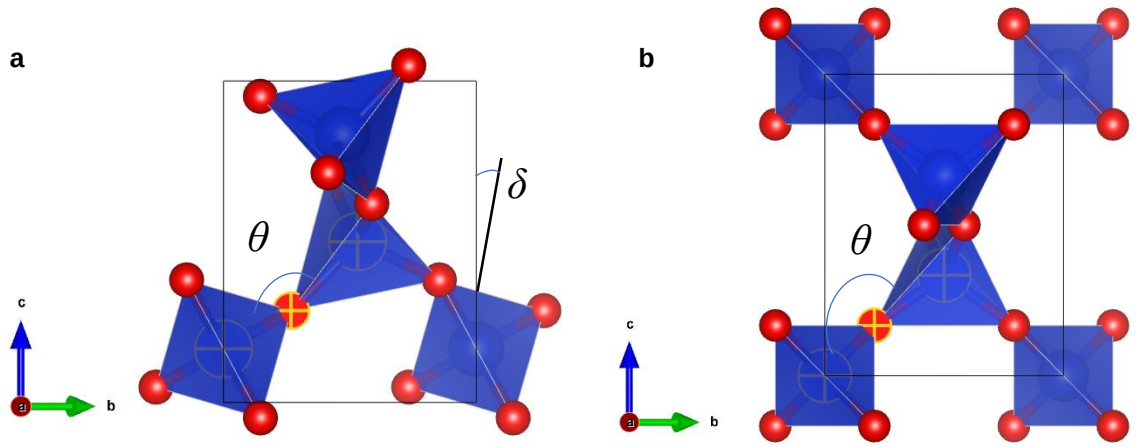

Fig. S4: Structures of a) α- and b) β-quartz characterized by the tetrahedral tilting angle (δ) and the $\widehat{SiOSi}$ intertetrahedral bridging angle (θ). Silicon and oxygen atoms are respectively shown blue and red spheres.

Table S1: ***c*/*a*** unit-cell parameter ratio, θ and δ-angles for α-, β-quartz, $BaZnO_2$ and $BaCoO_2$.

	α-quartz (291 K)	β-quartz (1012 K)	$BaZnO_2$	$BaCoO_2$
c*/*a	1.1	1.0916	1.1433	1.1483°
θ	143.6°	154°	152.3°	151.2°
δ	16.6°	0	10.14°	13.93°

Table S2: Bond Valence Sum (BVS), Coordination Number (CN), and the Bond Length of the Refined Structure of $P3_121$ $BaCoO_2$ at 400 K, obtained by the Rietveld Analysis of Neutron Data using the program FULLPROF Suite[11] using bond valence parameters[12]

Atom	BVS	CN	Bond length
Ba	1.778(19)	8	r(Ba-O)= 2.9004(33)
Co	1.939(31)	4	r(Co-O)= 1.9646(61)
O	1.858(29)	6	r(Co-O)+ r(Ba-O)=2.5884(44)

Magnetic properties of $BaCoO_2$

The magnetic susceptibility of the synthesized $BaCoO_2$ is reported in the Fig. S5 between 1.8 and 400 K; note that the secondary phases of CoO and $BaCoO_{2+\varepsilon}$ with antiferromagnetic ordering at ~ 290 K[13] and 220 K[9] respectively are weakly detected, Fig. S5a. One can see that there is a magnetic hysteresis between the ZFC and FC magnetic susceptibilities below 358 K, Fig. S5a. There is a maximum and an inflexion point in the ZFC magnetic susceptibility at 335 K, respectively. This is a signature of an antiferromagnetic order with a significant ferromagnetic component. This is confirmed by the magnetization curves of $BaCoO_2$, which show a weak hysteresis at 320 K, i. e. Fig. 5b below the phase transition temperature, whereas it is linear at 400 K. As can be seen in the inset of the Fig. 5a, there is an approximate linear variation for the inverse of the magnetic susceptibility between 365 K and 400 K which is characteristics of a Curie-Weiss law.

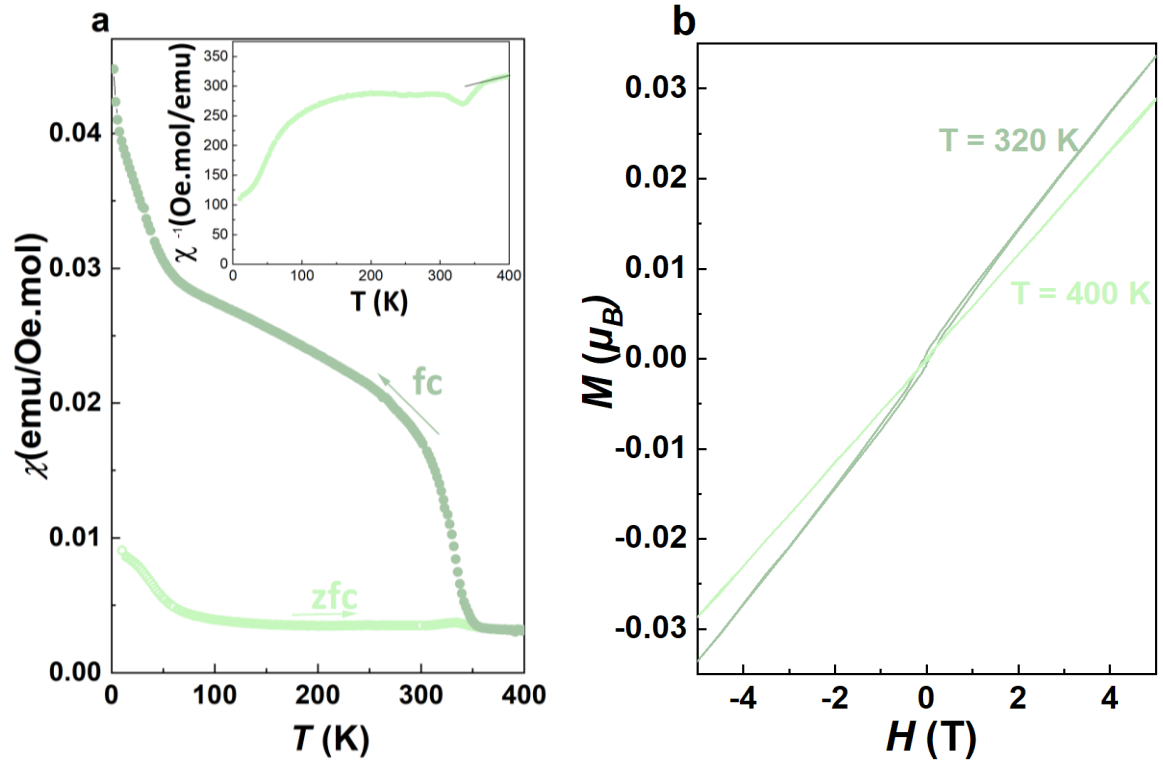

Fig. S5: Magnetic susceptibility of $BaCoO_2$. a) Zero field cooling (ZFC) and field cooling (FC, 100 Oe); Insert: Inverse of the ZFC magnetic susceptibility of $BaCoO_2$. b) Magnetization of $BaCoO_2$ at 320 K and 400 K.

One finds a Curie-Weiss temperature θ = -573(1) K and μ_{eff} = 4.95(5) μ_B. This confirms the antiferromagnetic character of the magnetic transition. In the case of Co^{2+} ion with a high spin $3d^7$ electronic configuration in an ideal tetrahedral environment and considering only the spin,

μ_{eff}^{spin} = 3.87 μ_B[14], which is smaller than the experimental fitted value. The difference can be explained by the existence of either spin orbit coupling and/or crystal field distortion of the observed CoO_4 tetrahedra in trigonal symmetry. Our experimental value is very close to that found for paramagnetic salts containing Co^{2+} ions (μ_{eff} = 4.9 μ_B)[15].

Resistivity of $BaCoO_2$

Fig. S6 shows the variation of sample resistivity as a function of the inverse of temperature. The measurements were performed under a vacuum better than 10^{-7} bar. Based on ohmicity tests, I=10 μA was determined to perform resistivity measurements. The study was carried out in the temperature range 300-700 K. From Fig. S6, we can assume that the resistivity of the sample is relatively insensitive to temperature changes up to T ~ 360K. Upon heating, a strong decrease in resistivity can be observed. The linear variation of log(ρ) vs 1/T is typical for a thermally activated conduction process. The activation energy of this process can be estimated as E_a = 520 meV. The resistivities of $BaCoO_3$ (Yamaura et al.)[16] and BSCF (Wei et al.)[17] are also plotted on Fig. S6. $BaCoO_2$ exhibits a much higher resistivity compared to $BaCoO_3$ at ambient temperature, but as its the activation process is more pronounced than that of $BaCoO_3$, the transport properties of both compounds would cross at about 973 K. The resistivity of $BaCoO_3$ may also be sensitive to the PO_2 as it is shown, for example, in BSCF, for which the oxygen conductivity participates to the transport properties, Fig. S6, as shown by a drop of the resistivity when measured in air. This means that one may assume a decrease of resistivity in $BaCoO_3$ if the oxygen stoichiometry decreases.

It is interesting to note that $BaCoO_2$ would present a similar resistivity to BSCF at about 1273 K based on these data. This comparison is important as $BaCoO_2$/$BaCoO_3$ are parent phases of BSCF and as the oxygen stoichiometry of BSCF in this temperature range is proposed to be from 2.3 to 2.6 with the cobalt being mostly in the 2+ state[18].

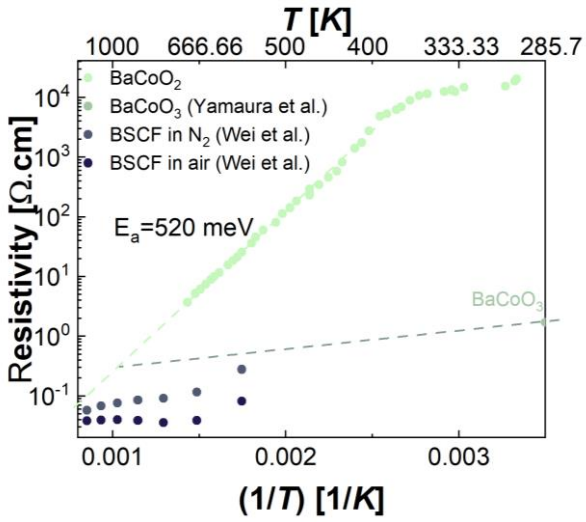

Fig. S6: Resistivity measurements of $BaCoO_2$. Arrhenius plot fitted in the 400-700 K range is shown. Resistivity measurements of $BaCoO_3$ (Yamaura et al.)[16] and BSCF (Wei et al.)[17] are shown for comparison. For $BaCoO_3$, the Arrhenius slope extracted from the data in the range 160 K < T < 300 K is also added.

Infrared of $BaCoO_2$

Infrared data were obtained in transmission geometry on a Bruker IFS 66 V Fourier transform spectrometer using a 6 μm mylar beamsplitter and a mercury discharge lamp. A Si-bolometer detector cooled at 4.6 K was used to probe the far-infrared domain. The $BaCoO_2$ sample was ground with polyethylene and compressed to form pellets of 13 mm diameter[19]. The spectral resolution was 4 cm^{-1}, and 128 scans were accumulated.

The infrared spectrum has been calculated via the Berry phase technique according to the reference[26]. As only the frequency position of bands and their intensities can be obtained using the harmonic approximation, we used a Lorentzian line shape and a constant linewidth fixed at 4 cm^{-1} to display the infrared spectrum in Fig. S7.

Fig. S7 shows experimental and calculated infrared spectra of $BaCoO_2$. Although the experimental data are rather broad, the simulated infrared spectrum of $BaCoO_2$ appears to be in qualitative agreement with the experimental one.

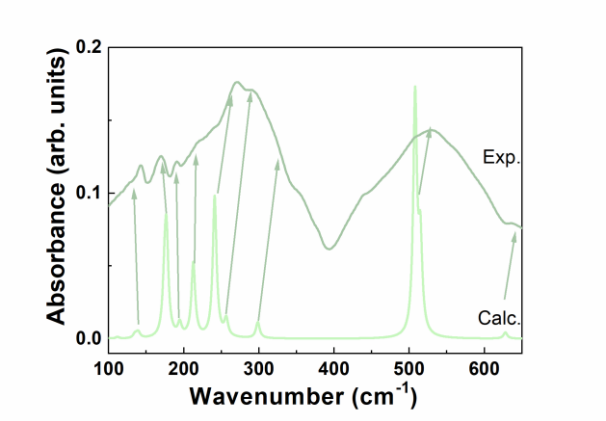

Fig. S7: Experimental and calculated spectra of $BaCoO_2$; arrows are added to see the correspondence between the calculated and the experimental bands

$BaCoO_{3-\delta}$

The 2H-$BaCoO_{3-\delta}$ structure was synthesized from a stoichiometric mixture of $BaCO_3$ and CoO under an oxygen flux (PO_2 = 1 bar) at 993 K for 4 hours and quenched in liquid nitrogen. Whereas X-ray diffraction data showed almost pure 2H-$BaCoO_{3-\delta}$ phase, Fig. S8a, neutron diffraction, Fig. S8b, permits to evidence the coexistence with the 12H-$BaCoO_{2.6}$ phase with a weight fraction ratio 87.8 and 12.2 % respectively. Neutron diffraction appears as the appropriate technique to probe the purity of the 2H-$BaCoO_{3-\delta}$ phase. It is highly important to note that the coexistence with the 12H-$BaCoO_{2.6}$ phase is probably inherent of such a high temperature synthesis as previous neutron data from the literature claiming a "2H-$BaCoO_{3-\delta}$ single phase" already contained the two most intense reflection of the $BaCoO_{2.6}$ phase (in Fig. 1 from this reference[27]) as shown by the arrows about 70° (2θ) in Fig. S8b.

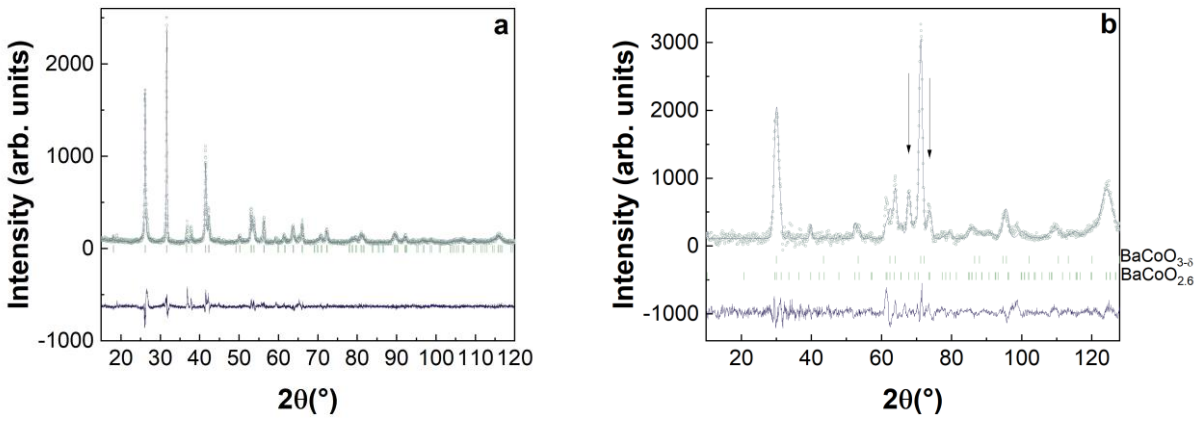

Fig. S8: Structural characterization of $BaCoO_{3-\delta}$ (a) using X-ray *K*-$Cu_{\alpha 1}$-radiation (Bragg R-factor: 8.3 %) and (b) neutron diffraction using λ=2.52 Å (Bragg R-factor: 3.71 %). Experimental, simulated data and difference are respectively shown using open dots, gray and blue lines. Vertical ticks describe the 2H-$BaCoO_{3-\delta}$ and 12H-$BaCoO_{2.6}$ phases (with their corresponding calculated weight fractions from Rietveld refinement: 87.8 and 12.2 %). The large background due to the use of amorphous silica crucible for this experiment was subtracted. The arrows highlight the two most intense reflection from the 12H-$BaCoO_{2.6}$ phase.

Structural evolution of $BaCoO_2$ in air as a function of temperature by neutron diffraction

$BaCoO_2$ is found to directly transform to the 2H-$BaCoO_{3-\delta}$ phase in air at about 523 K. Contrary to the BCO phase synthesized at high temperature, the 2H-hexagonal structure of BCO is obtained as a single phase without the presence of the 12H-$BaCoO_{2.6}$ phase as observed in Fig. S8b. More importantly, an antiferromagnetic order defined by k = (0,0,0.5) can be determined, Fig. S9. The magnetic structure has been determined using representation theory, considering the space group and Wyckoff position of the Co. The decomposition yields two irreducible representations allowed, and refinement shows that only one correctly reproduces the observed intensities. The magnetic structure consists of a helix with a magnetic moment in the ab plane that rotates 90° along the c axis. The refined magnetic moment of Co is 0.76(3)μ_B. This structure corresponds to a magnetic space group C_c2.When temperature is increasing BCO progressively transforms into $BaCoO_{2.6}$ phase. At the highest temperature reached, 1177 K on Fig. S10, the transition is not complete.

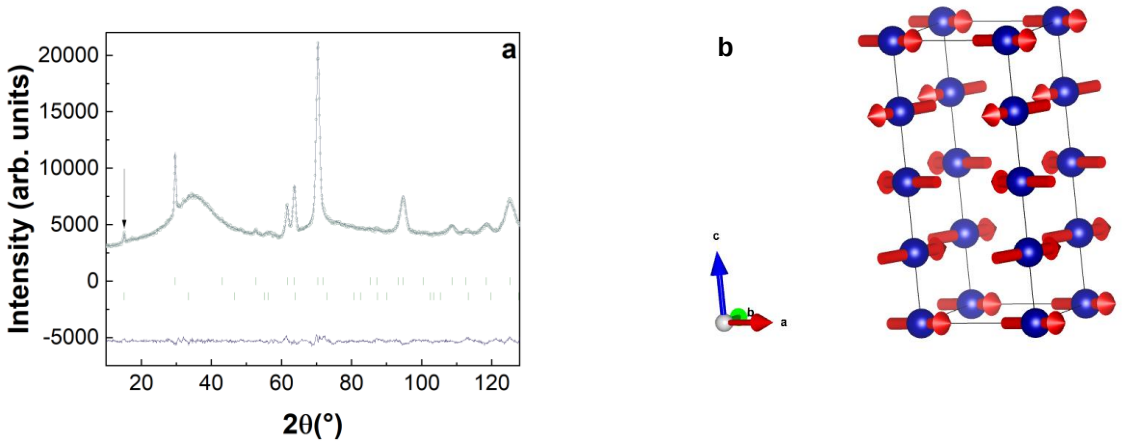

Fig. S9: Transformation in $BaCoO_{3-\delta}$. (a) Neutron diffraction data from $BaCoO_2$ phase heated in air at 623 K resulting in a $BaCoO_{3-\delta}$ pure phase. Note the additional reflection under the arrow which can be indexed using k = (0,0,1/2) propagation vector characterizing an antiferromagnetic structure. Vertical ticks from top-down in the corresponding Rietveld refinement indicates nuclear and magnetic reflections of $BaCoO_{3-\delta}$ phase. (b) In-plane rotation of the magnetic moment along ***c****, i.e. 0.76(3)μ_B/Co atom, characterizing the antiferromagnetic

structure of $BaCoO_{3-\delta}$ with magnetic space group C_c2. Nuclear *Bragg R-factor*=3.08 %, magnetic *R-factor=56.9 %*.

Note that in the present neutron diffraction study, the use of a λ=2.52Å wavelength, i.e. with a corresponding resolution up to 1.4 Å, did not permit the oxygen occupation to be refined; this parameter was therefore fixed to the value determined from the TGA measurements in Fig 4b.

Table S3: Bond Valence Sum (BVS), Coordination Number (CN), and the Bond Length of the Refined Structure of $P6_3/mmc$ $BaCoO_{3-\delta}$ at 523 K, obtained by the Rietveld Analysis of Neutron Data using the program FULLPROF Suite[11] using bond valence parameters[12]

Atom	BVS	CN	Bond length
Ba	1.846(6)	10.08	r(Ba-O)= 2.9211(11)
Co	3.210(12)	5.04	r(Co-O)= 1.8871(14)
O	2.006(11)	6	r(Co-O)+ r(Ba-O)= 2.5764(15)

Table S4: Bond Valence Sum (BVS), Coordination Number (CN), and the Bond Length of the Refined Structure of $P6_3/mmc$ $BaCoO_{3-\delta}$ at 702 K, obtained by the Rietveld Analysis of Neutron Data using the program FULLPROF Suite[11] using bond valence parameters[12]

Atom	BVS	CN	Bond length
Ba	2.054(67)	11.52	r(Ba-O)= 2.9315(109)
Co	3.772(147)	5.76	r(Co-O)= 1.8768(144)
O	2.022(113)	6	r(Co-O)+ r(Ba-O)= 2.5799(151)

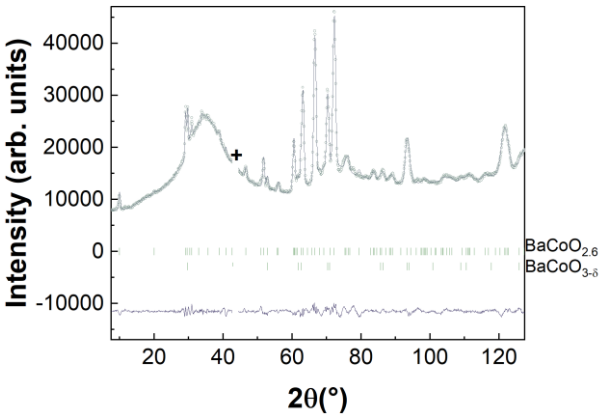

Fig. S10: Neutron diffraction data at 1177 K. At about 900-950 K, $BaCoO_{3-\delta}$ starts to transform into 12H- $BaCoO_{2.6}$ phase. At the highest temperature reached (1177 K), the 12H- $BaCoO_{2.6}$/ $BaCoO_{3-\delta}$ phase fraction reaches 70 %/30 %; vertical ticks show 12H- $BaCoO_{2.6}$ (*Bragg R-factor* =6.42 %) and $BaCoO_{3-\delta}$ (*Bragg R-factor* =5.45 %) reflections respectively. An excluded region **(+)** had to be used to remove the contribution from the sample environment during heating at such a temperature.

Structural evolution of $BaCoO_{3-\delta}$ in vacuum as a function of temperature by neutron diffraction

The starting $BaCoO_{3-\delta}$ neutron data for this structural study has already been shown in Fig. S8b. At about 1123 K, BCO starts to transform into the cubic $BaCoO_{2.2}$ phase, Fig. S11.

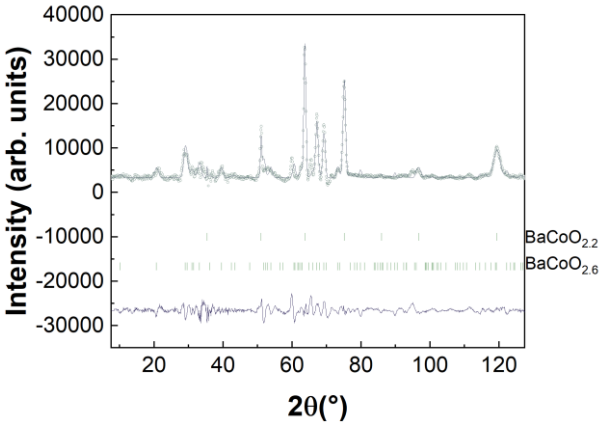

Fig. S11: Neutron diffraction data at 1193 K. At about 1123 K, the $BaCoO_{3-\delta}$ majority phase starts to transform into the cubic $BaCoO_{2.2}$ phase. Vertical ticks show $BaCoO_{2.2}$ (*Bragg R-factor* =5.5 %) and $BaCoO_{2.6}$ (*Bragg R-factor* =18.5 %) reflections respectively. The large background due to the use of amorphous silica crucible for this experiment was subtracted. The data quality does not permit to estimate accurate phase fractions.

1 Goldschmidt, V. M. The laws of crystal chemistry. *Naturwissenschaften* **14**, 477-485, doi:10.1007/bf01507527 (1926).

2 B. Raveau and M. Seikh , Cobalt Oxides: From Crystal Chemistry to Physics , Wiley VCH, 2012

3 Mentre, O. *et al.* BaCoO2.22: the most oxygen-deficient certified cubic perovskite. *Dalton Transactions* **44**, 10728-10737, doi:10.1039/c4dt03874f (2015).

4 Gushee, B. E., Katz, L. & Ward, R. THE PREPARATION OF A BARIUM COBALT OXIDE AND OTHER PHASES WITH SIMILAR STRUCTURES. *J. Am. Chem. Soc.* **79**, 5601-5603, doi:10.1021/ja01578a004 (1957).

5 Jacobson, A. J. & Hutchison, J. L. AN INVESTIGATION OF THE STRUCTURE OF 12HBACO02.6 BY ELECTRON-MICROSCOPY AND POWDER NEUTRON-DIFFRACTION. *J. Solid State Chem.* **35**, 334-340, doi:10.1016/0022-4596(80)90530-7 (1980).

6 Boulahya, K. *et al.* Ferromagnetism in Ba5Co5O14: A structural, transport, thermal, and magnetic study. *Phys. Rev. B* **71**, doi:10.1103/PhysRevB.71.144402 (2005).

7 Spitsbergen, U. THE CRYSTAL STRUCTURES OF BAZNO2, BACOO2 AND BAMNO2. *Acta Crystallographica* **13**, 197-198, doi:10.1107/s0365110x60000467 (1960).

8 Diatta, A., Rouquette, J., Armand, P. & Hermet, P. Density Functional Theory Prediction of the Second Harmonic Generation and Linear Pockels Effect in Trigonal BaZnO2. *J. Phys. Chem. C* **122**, 21277-21283, doi:10.1021/acs.jpcc.8b08174 (2018).

9 Waidha, A. I. *et al.* BaCoO2+: a new highly oxygen deficient perovskite-related phase with unusual Co coordination obtained by high temperature reaction with short reaction times. *Chemical Communications* **55**, 2920-2923, doi:10.1039/c8cc09532a (2019).

10 Waidha, A. I. *et al.* Structural, Magnetic and Catalytic Properties of a New Vacancy Ordered Perovskite Type Barium Cobaltate BaCoO2.67. *Chemistry-a European Journal* **27**, 9763-9767, doi:10.1002/chem.202101167 (2021).

11 Rodriguez-Carvajal, J. in *18th Conference on Applied Crystallography.* 30-36 (2001).

12 Brese, N. E. & Okeeffe, M. BOND-VALENCE PARAMETERS FOR SOLIDS. *Acta Crystallographica Section B-Structural Science* **47**, 192-197, doi:10.1107/s0108768190011041 (1991).

13 Tomiyasu, K., Inami, T. & Ikeda, N. Magnetic structure of CoO studied by neutron and synchrotron x-ray diffraction. *Phys. Rev. B* **70**, doi:10.1103/PhysRevB.70.184411 (2004).

14 B. N. Figgis, M. A. Hitchman, Ligand Field Theory and Its Applications, Special Topics in inorganic chemistry, Ed : Wyley-VCH, 2000.

15 Blundell, S. *Magnetism in Condensed Matter*. (OUP Oxford, 2001).

16 Yamaura, K. & Cava, R. J. Magnetic, electric and thermoelectric properties of the quasi-1D cobalt oxides Ba(1-x)La(x)CoO3 (x=0, 0.2). *Solid State Commun.* **115**, 301-305, doi:10.1016/s0038-1098(00)00188-5 (2000).

17 Wei, B. *et al.* Thermal and electrical properties of new cathode material Ba0.5Sr0.5Co0.8Fe0.2O3-delta for solid oxide fuel cells. *Electrochem Solid St* **8**, A428-A431, doi:10.1149/1.1951232 (2005).

18 Arnold, M., Xu, Q., Tichelaar, F. D. & Feldhoff, A. Local Charge Disproportion in a High-Performance Perovskite. *Chemistry of Materials* **21**, 635-640, doi:10.1021/cm802779f (2009).

19 Hermet, P. *et al.* Far- and Mid-Infrared of Crystalline 2,2‘-Bithiophene: Ab Initio Analysis and Comparison with Infrared Response. *The Journal of Physical Chemistry A* **109**, 1684-1691, doi:10.1021/jp045519m (2005).

20 Kresse, G. & Furthmuller, J. Efficiency of ab-initio total energy calculations for metals and semiconductors using a plane-wave basis set. *Computational Materials Science* **6**, 15-50, doi:10.1016/0927-0256(96)00008-0 (1996).

21 Kresse, G. & Hafner, J. Ab initio molecular dynamics for liquid metals. *Phys. Rev. B* **47**, 558-561, doi:10.1103/PhysRevB.47.558 (1993).

22 Perdew, J. P., Burke, K. & Ernzerhof, M. Generalized gradient approximation made simple. *Phys. Rev. Lett.* **77**, 3865-3868, doi:10.1103/PhysRevLett.77.3865 (1996).

23 Kresse, G. & Joubert, D. From ultrasoft pseudopotentials to the projector augmented-wave method. *Phys. Rev. B* **59**, 1758-1775, doi:10.1103/PhysRevB.59.1758 (1999).

24 Monkhorst, H. J. & Pack, J. D. Special points for Brillouin-zone integrations. *Phys. Rev. B* **13**, 5188-5192, doi:10.1103/PhysRevB.13.5188 (1976).
25 Dudarev, S. L., Botton, G. A., Savrasov, S. Y., Humphreys, C. J. & Sutton, A. P. Electron-energy-loss spectra and the structural stability of nickel oxide: An LSDA+U study. *Phys. Rev. B* **57**, 1505-1509, doi:10.1103/PhysRevB.57.1505 (1998).
26 Hermet, P. *et al.* Far- and mid-infrared of crystalline 2,2′-bithiophene:: Ab initio analysis and comparison with infrared response. *J. Phys. Chem. A* **109**, 1684-1691, doi:10.1021/jp045519m (2005).
27 Nozaki, H. *et al.* Antiferromagnetic spin structure in BaCoO3 below 15 K determined by neutron and mu+SR. *J Phys Chem Solids* **68**, 2162-2165, doi:10.1016/j.jpcs.2007.08.059 (2007).